Microwave Diathermy for Deep Heating Therapy of Knee Joint

Asmaa E. Farahat[1, *], Heba M. Kahil[2], and Khalid F. A. Hussein[1]

Abstract—This study proposes the idea of a thermotherapy device for the treatment of human knee joint disorders by the thermal effect of microwave radiation. The device is composed of a circular array of dipole antennas operating at 2.45 GHz. A high resolution three dimensional geometric, electric, and thermal model for a human right knee is constructed. Electromagnetic simulations are performed to calculate the specific absorption rate (SAR) distribution within the tissues of the human knee using the finite difference time domain (FDTD) method. The SAR distributions are calculated for four and eight elements circular arrays. The FDTD is applied to calculate the rise in temperature within different tissues of the human knee due to the exposure to different levels of heating microwave power. The effect of the tissue thermoregulatory response on the temperature rise is investigated for each individual tissue type. Moreover, the dependence of the induced steady state rises in tissue temperatures on the absorbed SAR is studied in the case of the SAR at a point in the muscle tissue (local SAR), and the SAR averaged over 1 g ($SAR_{1\,g}$) and over 10 g ($SAR_{10\,g}$). The rise in temperature distribution due to radiation from the circular array of dipoles is calculated at different cross sections.

1. INTRODUCTION

Thermotherapy is a deep heating modality that increases the blood flow in tissues through blood vessels dilation. This dilation will in turn increase the pressure of the capillaries, the permeability of the cell membrane, and the rate of metabolism, causing a rapid transfer of more nutrients from the blood across cell membranes. These actions can reduce the pain and promote healing [1]. Microwave-thermotherapy and the health effects of human exposure to electromagnetic waves have attracted electromagnetic researchers for the last two decades and up till now [2–7]. It has been shown that deep heating therapy via microwave diathermy relieves pain and improves physical function in patients with knee osteoarthritis [8].

The heat induced within tissues due to electromagnetic exposure is governed by the specific absorption rate (SAR) at each tissue. SAR is the rate at which the electromagnetic energy is deposited in the biological tissue expressed in watts per kilogram (W/kg). Each tissue type absorbs a specific amount of energy according to its electric conductivity and density.

Many studies in the past applied the finite difference time domain (FDTD) method for calculating the power absorbed in a human body exposed to electromagnetic fields in terms of SAR. The FDTD method is simple to formulate, has a wide frequency response for one calculation, can simulate different types of materials, and is suitable for composite geometries. Biological tissues are lossy, heterogeneous, and have finite conductivities. They are also dispersive as their electric conductivity and relative permittivity vary with the frequency. The level of the microwave power decreases as the electromagnetic wave penetrates deeper in the biological tissue because it loses its power in the form of heat dissipation.

The relation between the absorbed power and the temperature rise in the tissue concerned is not straightforward. Temperature distributions in tissue during radio frequency exposure can be measured

* Corresponding author: Asmaa Elsayed Farahat (e_asma_e@yahoo.com).
[1] Microwave Engineering Department, Electronics Research Institute (ERI), Cairo, Egypt. [2] Biophysics, Department of Physics, Faculty of Science, Ain Shams University, Cairo, Egypt.

by solving the equation of bio-heat transfer [9–11]. Firstly the electric field distribution due to the external source of radiation is calculated. The electric and thermal parameters are assigned to the cells of the model, and the SAR distribution is obtained. The suitable boundary conditions are then applied to calculate the tissue temperature distribution.

Knee joint is subjected to many disorders which are frequently treated by microwave hyperthermia [12, 13]. In this part of the human body, many types of biological tissues are confined to a relatively small region. This arrangement allows the study of the response of different tissue types to electromagnetic radiation.

The present study calculates the SAR distributions within the tissues of the human right knee due to electromagnetic radiation from a single dipole and circular array of four and eight dipoles. The temperature rise in each tissue of the knee due to a single dipole is calculated for different SAR values using the Bio-Heat equation (BHE). Using a single dipole in the study of the temperature rise in tissues is because a wide range of SAR values is obtained for the same tissue type in a single simulation. If more than one dipole is used, SAR values will almost be homogenous or vary in small range, and hence more simulations are needed at different input power levels to get a wide variety of SAR values. The parameters that influence the temperature rise, namely, the absorbed power by the concerned tissue and by the surrounding area, the thermal characteristics of the considered and neighbouring tissues, the different heat exchange mechanisms, and finally the thermoregulatory response, are considered.

2. CONSTRUCTION OF THE GEOMETRIC MODEL OF THE KNEE

Three dimensional model for the knee is constructed from two dimensional images representing photographs of a human male right knee adopted from the US National Library of Medicine. The images of the US National Library of Medicine are in JPEG format. Each image is converted into bitmap (BMP) image and then discretized into 100×100 cells. A total of 100 sections are used to construct the 3D model. From the human adult male anatomy for the right knee, the FDTD cell size is set to $0.1289 \times 0.1289 \times 0.1289\,\mathrm{cm}^3$. The model is built up of eight tissue types, namely, skin, bone, muscle, tendon, fat, connective tissue, body fluid (synovial fluid), and cartilage. An axial cross section is presented in Figure 1(a) showing the femur condyle, patella, plantaris semimembranosus muscle, biceps femoris, sartorious and vastus medialis muscle. The constructed FDTD cross section corresponding to the anatomy section in Figure 1(a) is shown in Figure 1(b).

(a)   (b)
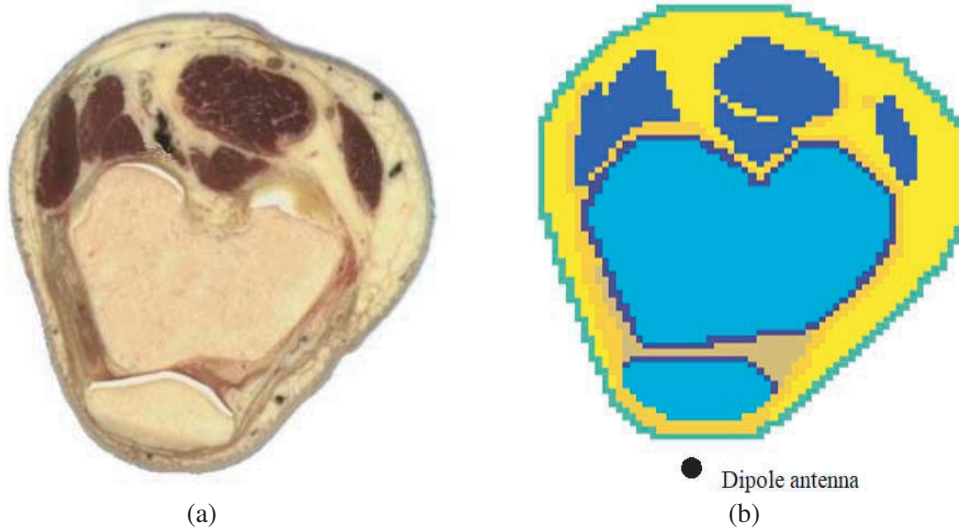
Figure 1. (a) Axial anatomical cross section for the knee. (b) The constructed FDTD cross section corresponding to that in Figure 1(a).

In Figure 2(a), an anatomical sagittal cross section of the knee is illustrated, and in Figure 2(b), the corresponding constructed FDTD section is presented.

(a) (b)
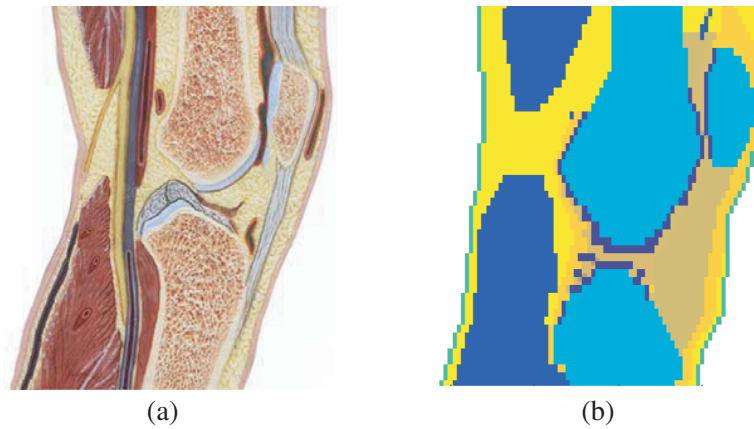
Figure 2. Sagital anatomic cross section and the corresponding representation in the FDTD model of the knee. (a) Sagittal anatomic cross section. (b) FDTD gemetric model of the sagittal cross section.

The electric properties, namely the relative permittivity and the electric conductivity, and the density for each tissue type are given in Table 1 [14].

The FDTD method is applied to the computation of the electric fields, and then the SAR is calculated inside the knee tissues due to electromagnetic exposure. The FDTD lattice is formed of cubic cells; 121 cells in the x-direction, 121 cells in the y-direction, and 121 cells in the z-direction.

Table 1. Electric properties and density for each tissue type in the knee.

Tissue type	ρ (kg/m^3)	ϵ_r	σ (ohm^{-1}m^{-1})
Bone	1900	18.548	0.805
Body fluid	1000	68.208	2.47
Cartilage	1100	38.77	1.7559
Connective tissue	923	10.820	0.2679
Fat	918	5.280	0.104
Muscle	1040	52.729	1.7338
Skin	1050	38.007	1.464
Tendon	1040	43.121	1.684
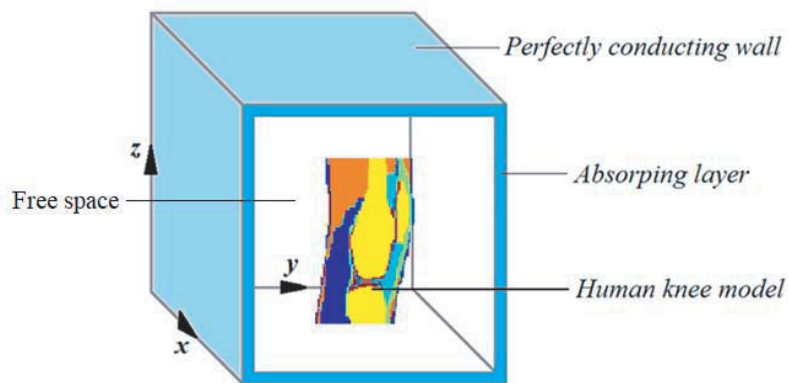
Figure 3. FDTD model for the SAR computation in the knee tissues.

The cell side length is 0.1289 cm. The boundaries of the FDTD volume are terminated with uniaxial perfectly matched layer (UPML) [15] composed of eight layers. The volume outside the knee model is assumed to be free space. Each FDTD cell in the model is assigned specific electric conductivity, permittivity, and mass density, given in Table 1 for the knee tissues or assigned the values of the free space. The FDTD model is shown in Figure 3.

The source of the electromagnetic radiation involved here is an array of half wavelength dipole antenna elements operating at 2450 MHz, and each array element is represented by a thin wire model [16]. The dipole is excited across an infinitesimal gap at the dipole center by a sinusoidal voltage signal. The dipoles are placed parallel to the sagittal axis of the knee in a vertical position.

3. SAR CALCULATION USING FDTD

The SAR is the quantity responsible for the temperature rise in biological tissues due to electromagnetic exposure. In order to calculate the SAR, the internal fields at each point inside the knee tissues are obtained, and the SAR is evaluated directly from the steady state electric field as,

$$\text{SAR} = \frac{\sigma |E|^2}{2\rho} \tag{1}$$

which can be written in discrete form as

$$\begin{aligned}
\text{SAR}(i,j,k) &= \frac{\sigma(i,j,k) \left(\left| \hat{E}_x(i,j,k) \right|^2 + \left| \hat{E}_y(i,j,k) \right|^2 + \left| \hat{E}_z(i,j,k) \right|^2 \right)}{2\rho(i,j,k)} \\
&= \frac{\sigma(i,j,k) |\hat{E}(i,j,k)|^2}{2\rho(i,j,k)} \tag{2}
\end{aligned}$$

where $\hat{E}(i,j,k)$ is the amplitude of the steady state total electric field at the cell with the indices (i,j,k), $\sigma(i,j,k)$ the conductivity, and $\rho(i,j,k)$ the mass density of the tissue filling the same cell.

4. EVALUATION OF THE TEMPERATURE RISE IN THE KNEE TISSUES

Explicit formulations of the BHE have been developed to study the thermal responses in anatomically accurate body models [17, 18]. In these studies, only limited body regions were considered, and thermoregulation mechanisms were neglected. In the present work, convection, radiation, and evaporation boundary conditions are applied, and thermoregulatory responses are considered. In solving the thermal problem, we attempted to apply the most realistic initial boundary conditions. A complete thermal model of the human knee has been implemented. The Pennes BHE is employed to calculate the temperature rise within the knee tissues [19]. Convection, radiation, and evaporation boundary conditions are applied [20–22]. The effect of the thermoregulatory system has been considered as well. The FDTD method is used to solve the BHE in its discrete form. The three dimensional space is discretized into cuboidal voxels, each of size Δx, Δy, Δz. The discrete form of the BHE is given as,

$$\begin{aligned}
T_{i,j,k}^{n+1} &= T_{i,j,k}^n + \frac{k_{i,j,k}\Delta t}{\Delta^2 m_{i,j,k}C_{i,j,k}} \left(T_{i+1,j,k}^n + T_{i-1,j,k}^n + T_{i,j+1,k}^n + T_{i,j-1,k}^n + T_{i,j,k+1}^n + T_{i,j,k+1}^n \right. \\
&\quad \left. + T_{i,j,k-1}^n - 6T_{i,j,k}^n \right) \Delta^3 + \frac{\Delta t}{m_{i,j,k}C_{i,j,k}} A_o \Delta^3 + \frac{\Delta t}{C_{i,j,k}} SAR_{i,j,k} \\
&\quad + \frac{\Delta t}{m_{i,j,k}C_{i,j,k}} B_{i,j,k} \left(T_b - T_{i,j,k} \right) \Delta^3 \\
&\quad - \frac{\Delta t}{m_{i,j,k}C_{i,j,k}} \left(H_{RAD_{i,j,k}} + H_{CONV_{i,j,k}} + H_{EVAP_{i,j,k}} \right) \tag{3}
\end{aligned}$$

where, $T_{i,j,k}$ is the instantaneous tissue temperature (°C); $m_{i,j,k}$ is the mass of the tissue for the voxel i, j, k (kg) which can be computed from the product of the density $\rho_{i,j,k}$ and the voxel volume $V_{i,j,k}$; $C_{i,j,k}$ is the specific heat of the tissue (J/°C kg); $k_{i,j,k}$ is the thermal conductivity of tissue (W/°C·m).

A cubic voxel is used in the simulations such that $\Delta x = \Delta y = \Delta z = \Delta$, $V_{i,j,k}$ is the volume of the voxel (m^3) (equal to the product of $\Delta x \times \Delta y \times \Delta z$, the FDTD cell size in the x, y, z directions, respectively; $H_{RAD_{i,j,k}}$ is the radiation heat loss per unit volume from peripheral tissue (W/m^3); $H_{CONV_{i,j,k}}$ is the convection heat loss per unit volume from peripheral tissue (W/m^3); $H_{EVAP_{i,j,k}}$ is the evaporation heat dissipation per unit volume (W/m^3); T_b is the temperature of arterial blood entering the tissue ($^\circ$C). It should be noted that B is the constant which is defined as a term associated with blood flow $(J/s \cdot m^3 \cdot {}^\circ C)$ equal to the product of $b_{f_{i,j,k}}$ and C_b, where $b_{f_{i,j,k}}$ is the blood flow rate $kg/m^3 s$, and C_b is the specific heat of the blood $(J/^\circ C \cdot kg)$.

4.1. Calculation of the Parameters of the BHE

The radiation heat loss per unit volume from peripheral tissue, H_{RAD}, is calculated from the Stefan-Boltzman formula [20]

$$H_{RAD} = \varepsilon' \delta A_{eff} \left[T_{skin} + 273 \right]^4 - \left[T_{air} + 273 \right]^4 \tag{4}$$

where $\delta = 5.67 \times 10^{-8}\,W/(m^2 K^4)$ is the Stefan-Boltzman constant; $\varepsilon' \approx 0.98$ is the emissivity of the skin; A_{eff} is the area of the skin that is effective in radiating heat (m^2); T_{skin} is the temperature of the skin ($^\circ$C); and T_{air} is the ambient air temperature (assumed to be 25°C for current calculations).

The convection heat loss, H_{CONV}, from the body is given by

$$H_{CONV} = h_{CONV} A_{eff} \left(T_{skin} - T_{air} \right) \tag{5}$$

where $h_{CONV} = 2.7\,W/(m^2\,^\circ C)$ is the convection heat transfer coefficient.

The evaporation heat loss, H_{EVAP}, due to insensible perspiration from the surface voxel is given by [23].

$$H_{EVAP} = k_{EVAP} A_N \left(P_{w,skin} - P_{w,air} \right) \tag{6}$$

where $k_{EVAP} = 0.35\,W/m^2 \cdot mmHg$ is the evaporation coefficient; $P_{w,skin}$ and $P_{w,air}$ are vapor pressures of water at skin and air, respectively expressed in mmHg; A_N is the area of the voxel exposed to air (m^2).

The vapour pressure of water over the range of roughly 27°C–37°C can be presented well by

$$P_{w,skin} = 1.92 T_{skin} - S \tag{7}$$

where S is a constant equals to 2.53 mmHg.

The Von Neumann's stability criterion correlates the time step to the space step and other tissue constants to guarantee the stability of the numeric solution [24].

$$\Delta t \leq \frac{2\rho C \Delta^2}{12K + B \Delta^2} \tag{8}$$

Equation (8) can be simplified according to [25],

$$\Delta t \leq \frac{\rho C \Delta^2}{6K} \tag{9}$$

The Von Newman stability criterion Equation (9) is applied to yield a time step of 0.3 seconds.

4.2. Simulating the Tissue Thermoregulatory Control

The blood flow rate supplying a certain tissue is a function of the tissue temperature; it increases to cool the heated tissue by convection. The dependence of the temperature dependent constant related to blood flow rate $B(r,T)$ on the tissue temperature T is proposed in [26], where $B(r,T)$ is expressed as follows.

$$B(r, T(r)) = B(r), \quad T(r) \leq 39^\circ C \tag{10}$$

$$B(r, T(r)) = B(r) \left[1 + S_B \left(T(r) - 39 \right) \right], \quad 39^\circ C < T(r) < 44^\circ C \tag{11}$$

$$B(r, T(r)) = B(r) \left[1 + 5 S_B \right], \quad T(r) \geq 44^\circ C \tag{12}$$

where $B(r)$ is the tissue dependent constant related to blood flow rate stated in Table 2 and S_B is a constant equal to $0.8°C^{-1}$.

Each FDTD cell in the model is assigned specific thermal parameters. The coefficient of thermal conductivity K, the specific heat C, a constant related to blood flow B, and the basal metabolic rate A_o [27–30] are given in Table 2.

Table 2. Knee tissues thermal parameters.

Tissue type	C (J/kg°C)	K (J/s·m³°C)	A_o (J/s·m³)	B (J/s·m³°C)
Bone	1300	0.4	289.5	1000
Body fluid	4200	0.62	0	0
Cartilage	3500	0.47	1600	9000
Connective tissue	2500	0.25	300	520
Fat	2500	0.25	300	520
Muscle	3600	0.5	703.5	2700
Skin	3500	0.42	1620	8652
Tendon	3300	0.41	1600	9000

5. NUMERICAL RESULTS AND DISCUSSIONS

The electric field inside the knee tissues is calculated using the FDTD method, and the SAR distribution is obtained due to radiated electromagnetic fields from a single dipole antenna and from a circular array of four and eight dipole elements. In the following sections, the electric field and SAR distributions are obtained due to microwave radiation from a single dipole and a circular arrays of four and eight dipole antennas placed surrounding the knee. In all cases, the distribution of the electric field and SAR is drawn in two main planes, the axial and sagittal cross-sections. The two planes are shown in Figure 4 relative to the knee model. The induced temperature rise as a result of microwave exposure from one dipole is investigated taking into consideration the thermoregulatory mechanism.
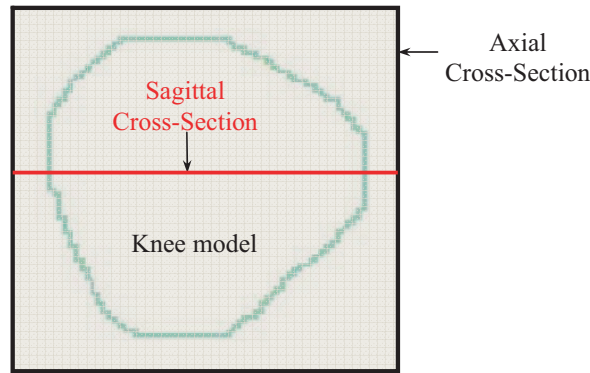
Figure 4. Definition of the axial and sagittal cross sections.

5.1. E-Field and SAR Distributions due to a Single Dipole

A single dipole is placed in front of the knee in the location indicated in Figure 1(b). A unit voltage is applied across an infinitesimal gap at the dipole centre. The electric field distributions in the middle axial and sagittal cross sections are shown in Figure 5. The corresponding SAR distributions are shown in Figure 6.
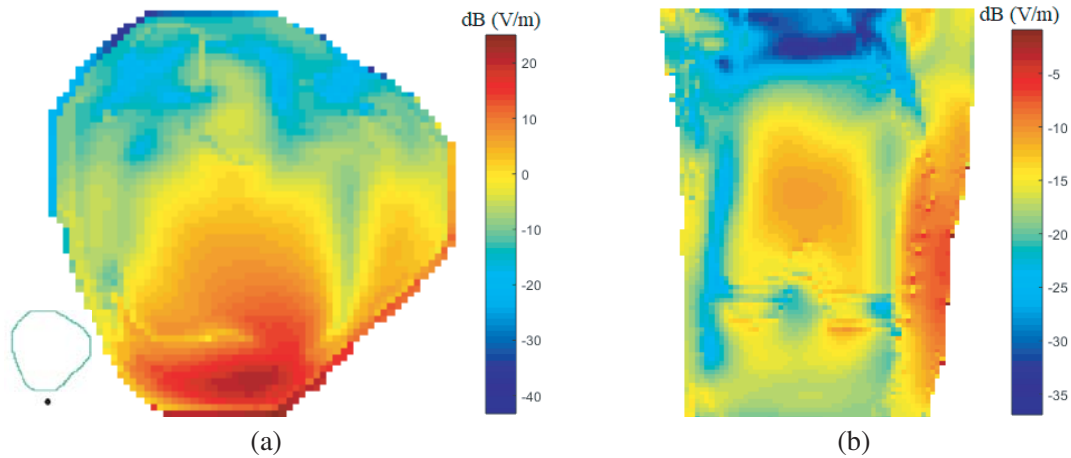
Figure 5. Electric field distribution in the middle (a) axial and (b) sagittal, cross sections of the knee model due to a single dipole placed in front of the patella.
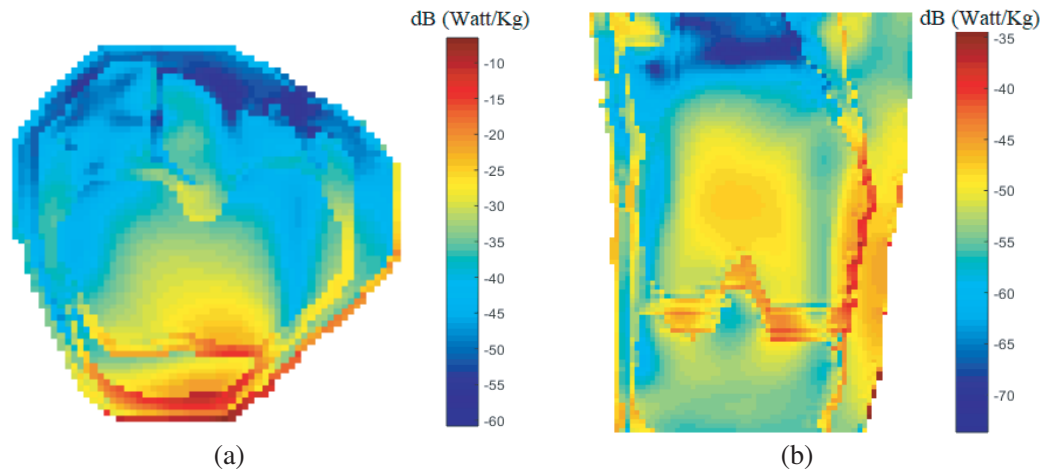
Figure 6. SAR distributions in the middle (a) axial and (b) sagittal, cross sections of the knee model due to a single dipole placed in front of the patella.

5.2. E-Field and SAR Distributions due to Radiation from Circular Array of 4 Dipoles

This section presents the plots for the electric field and SAR distribution inside the knee tissues due to electromagnetic exposure from a circular array of four dipole antennas. The circular array surrounds the knee with the dipoles placed parallel to the sagittal axis of the knee as shown in Figure 7. Each two adjacent dipoles are separated by 90°, i.e., the dipoles are placed at angles (0°, 90°, 180°, and 270°) on the circumference of a circle of diameter 11.6 cm. Each dipole is excited by a unit voltage sinusoidal signal applied across the infinitesimal gap at the dipole centre. The operating frequency is 2.45 GHz.

The electric field distributions in the middle axial and sagittal cross section of the model are presented in Figure 8(a) and Figure 8(b), respectively. The computed SAR distributions in the same cross sections are shown in Figures 9(a) and 9(b).

5.3. E-Field and SAR Distributions due to Radiation from Circular Array of 8 Dipoles

The source of microwave radiation is a circular array of eight dipoles arranged equally on the circumference of a circle with diameter 11.6 cm, placed around the knee model. Each two adjacent dipoles are separated by an angle 45°, i.e., the dipoles are placed at angles (0°, 45°, 90°, 135°, 180°,
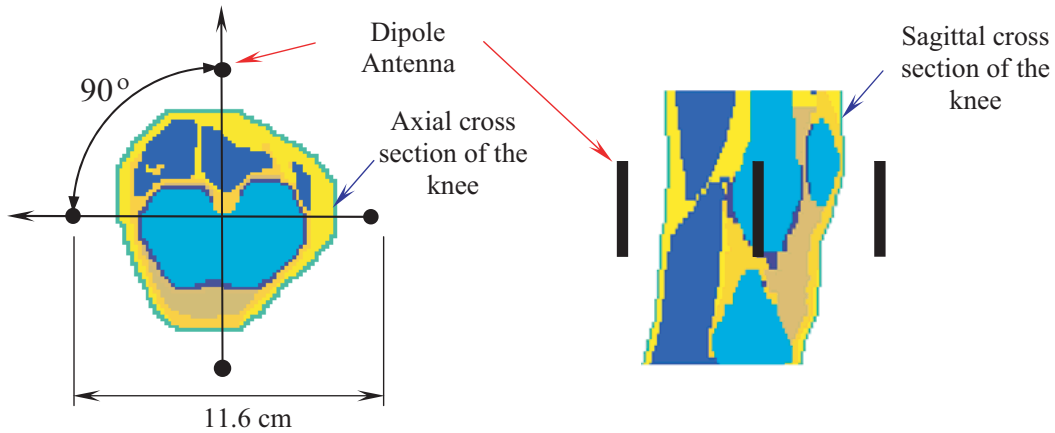
Figure 7. Circular array of four dipoles surrounding the knee.
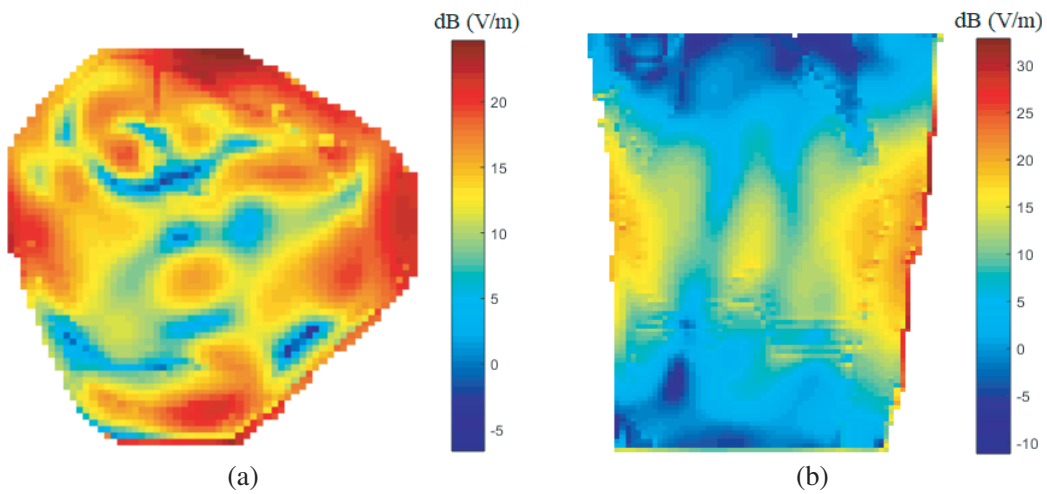
Figure 8. Electric field distributions in the middle (a) axial and (b) sagittal, cross sections of the knee model due to a circular array of four dipoles placed around the knee.
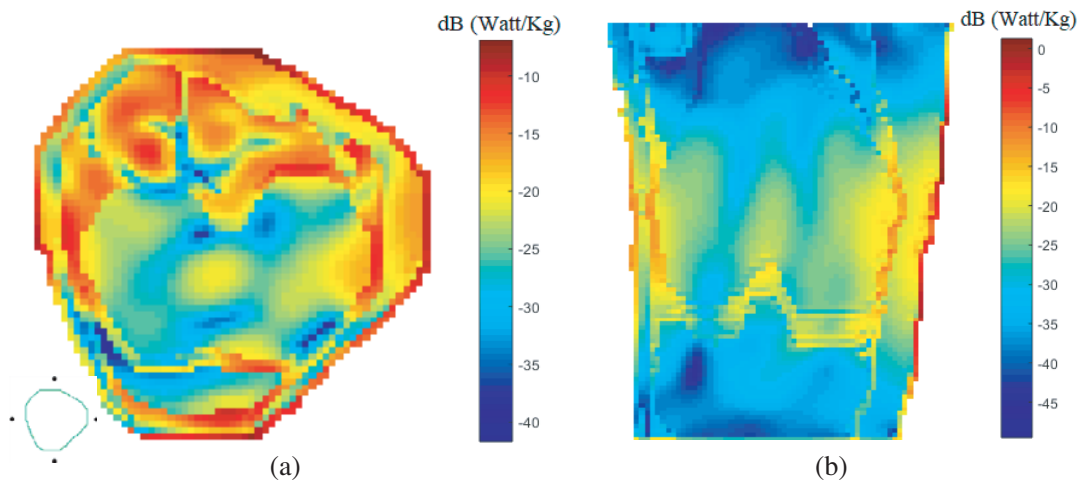
Figure 9. SAR distributions in the middle (a) axial and (b) sagittal, cross sections of the knee model due to a circular array of four dipoles placed around the knee.
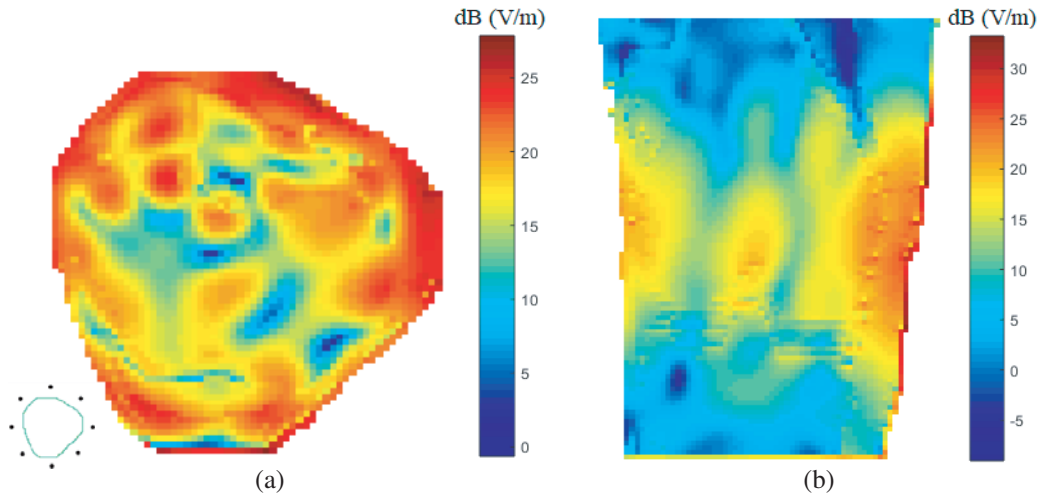
Figure 10. Electric field distributions in the middle (a) axial and (b) sagittal, cross sections of the knee model due to a circular array of eight dipoles placed around the knee.
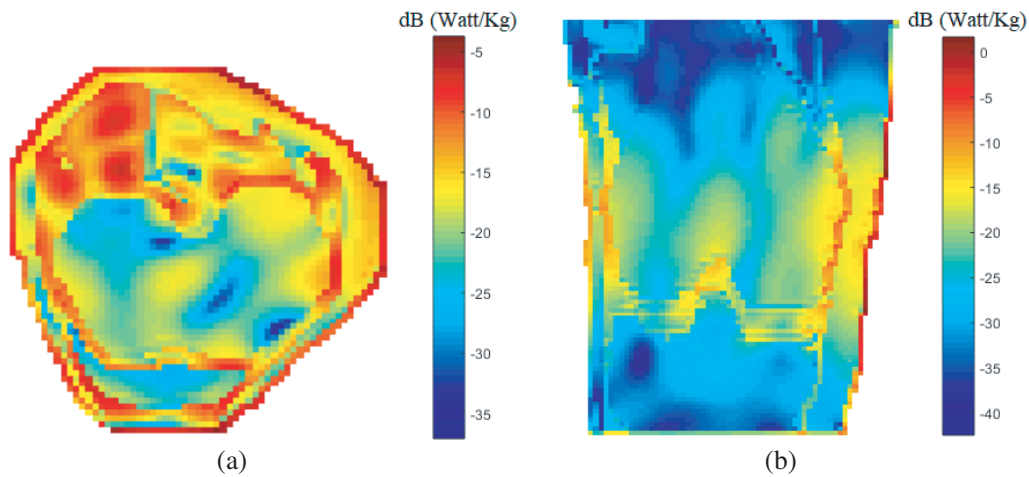
Figure 11. SAR distributions in the middle (a) axial and (b) sagittal, cross sections of the knee model due to a circular array of eight dipoles placed around the knee.

$225°$, $270°$, $315°$). The excitation for each dipole is a unit voltage sinusoidal signal across an infinitesimal gap at the centre of the dipole. The electric field distributions in the middle axial and sagittal cross sections are shown in Figures 10(a) and 10(b), respectively. The corresponding SAR distributions in the same sections are shown in Figures 11(a) and 11(b).

5.4. Steady State Initial Temperature Distribution

Solving the BHE to obtain the rise in temperature due to the exposure to electromagnetic energy requires the knowledge of the initial tissue temperature. The BHE Equation (3) is solved for 4000 time steps (total exposure time is 20 min). Air temperature is assumed to be $25°C$, arterial temperature $36°C$, and initial tissue temperature $36.2°C$. Figure 12 shows the initial steady state temperature distribution with the skin excluded from the figure scale to enhance the resolution to show the minor differences in temperature between different tissue types. The skin temperature is far lower. It is in the range of 27.7 to $30.09°C$. This low initial temperature is attributed to the fact that the skin is in contact with air ($25°C$) with which it exchanges heat by convection, radiation, and evaporation in addition to the rest of heat exchange mechanisms available for all tissues.
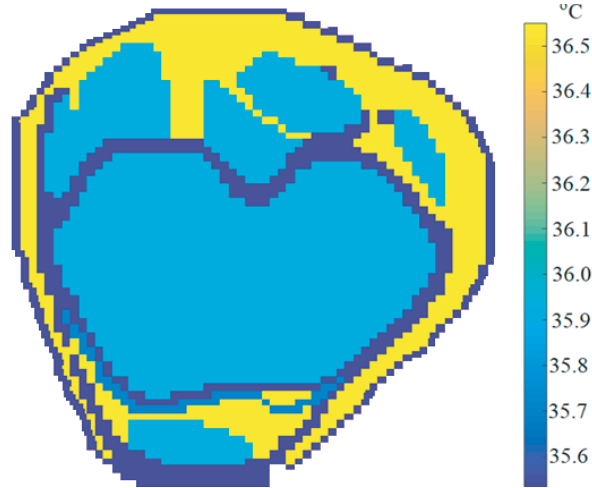
Figure 12. Initial temperature distribution in the cross section in the knee presented in Figure 2(b) excluding skin.

5.5. Effect of Thermoregulatory Response on the Tissue Temperature Rise

The effect of thermoregulatory response on the tissue temperature rise as stated by Equations (11)–(13) is investigated in this section. Figure 13 depicts the relation between the rise in tissue temperature (the difference between the instantaneous temperature $T_{i,j,k}$ and the initial tissue temperature stored in the computer memory) and the exposure time for muscle tissue exposed to electromagnetic radiation from a dipole antenna placed outside the knee and close to the skin parallel to the knee sagittal axis in the position shown in Figure 1(b). The dotted curve in Figure 13 represents the temperature rise under the assumption of the absence of the thermoregulatory response. In this case, there is a linear dependence of temperature rise on time for short exposure duration. The solid curve represents the rise in tissue temperature with time in the presence of thermoregulatory response. First, the two curves coincide, showing a linear rise in temperature with time. When the temperature rises to 39°C which is the threshold to trigger thermoregulatory response, it is found that the solid curve tends to have a lower slope and reaches steady state temperature after a time that depends on the tissue type and the exposure conditions.
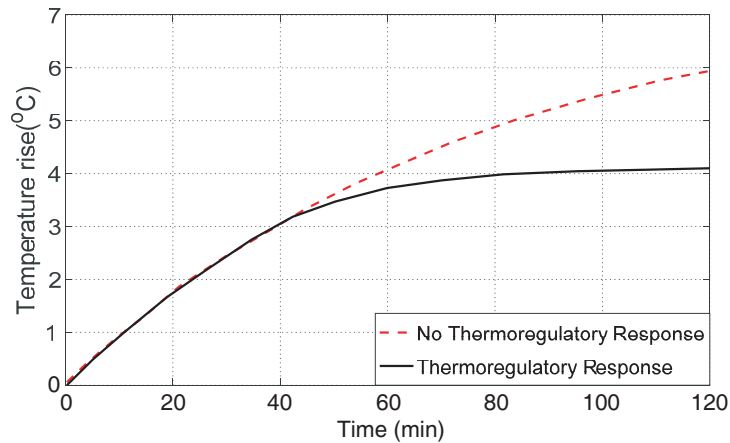
Figure 13. Effect of the thermoregulatory response on the temperature rise in muscle tissue.

The case in which thermoregulatory response is considered is a more realistic case, and hence it is applied onwards.

5.6. Temperature Rise with Time for Various Tissue Types

Under the effect of electromagnetic field and using the BHE, the temperature $T_{i,j,k}$ is calculated for each voxel of the knee as a function of time for exposure durations ranging from 120 to 240 min for different levels of radiated powers which correspond to different values of SAR. Figure 14 shows the variation of the temperature with time inside the knee for the muscle tissue by placing a dipole antenna in the position indicated in Figure 1(b). Using a single dipole in the study of the temperature rise in tissues is because a wide range of SAR values is obtained for the same tissue type in a single simulation. If more than one dipole is used, SAR values will almost be homogenous or vary in small range, and hence more simulations are needed at different input power levels.
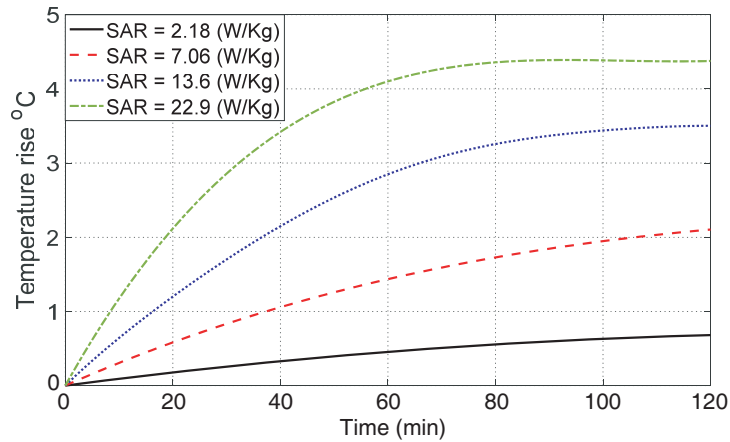
Figure 14. Temperature rise with time for muscle tissues subjected to different values of SAR.

The temperature-time relations shown in Figures 15 to 20 are obtained for different tissue types in the human right knee, due to a dipole antenna placed at the position indicated in Figure 1.
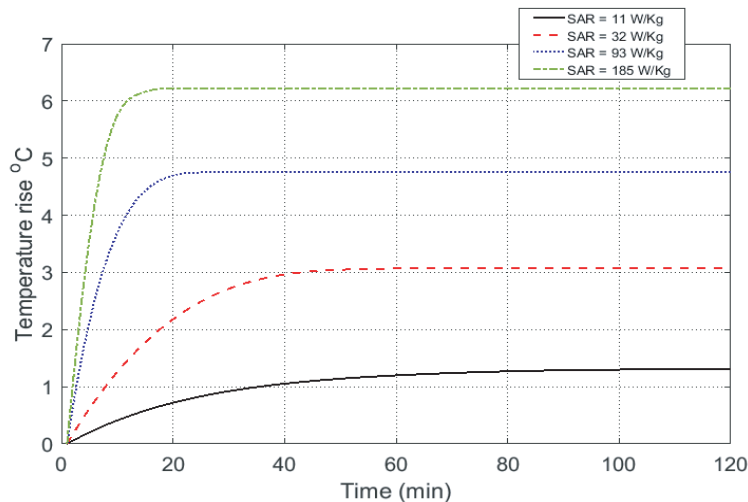
Figure 15. Temperature rise with time for tendon tissues subjected to different values of SAR.

It can be noticed from the results presented in Figures 14–20 that the six tissue types — muscle, tendon, fat, skin, cartilage, and bone — reach steady state temperature after a corresponding period of time depending on the tissue type. The steady state temperature is reached after different exposure durations for different SAR values. In the six plots, the transient temperature rise shows a linear
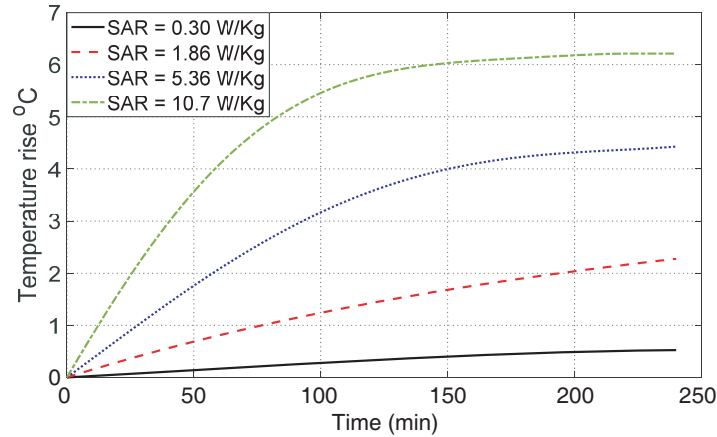
Figure 16. Temperature rise with time for fat tissues subjected to different values of SAR.
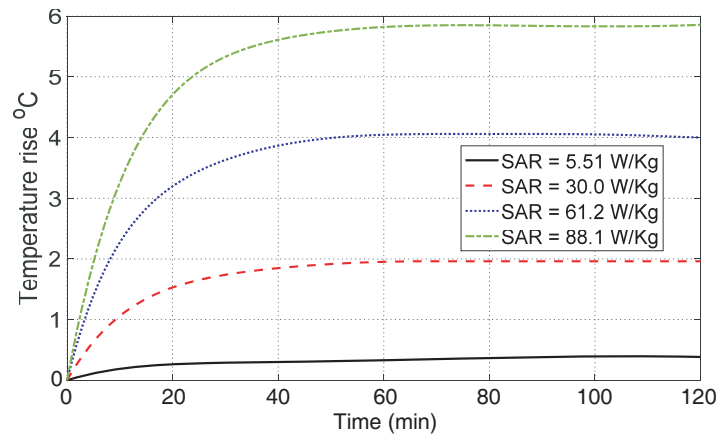
Figure 17. Temperature rise with time for skin tissues subjected to different values of SAR.
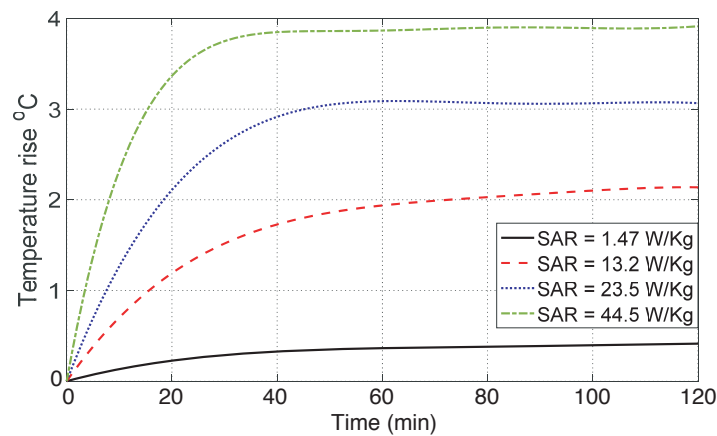
Figure 18. Temperature rise with time for cartilage tissues subjected to different values of SAR.

dependence on SAR for short exposure duration. After a certain time that depends on the tissue parameters and exposure conditions, the temperature stabilizes at a certain steady state value. Tissues lose the excess heat by conduction to neighbouring tissues, radiation, evaporation to air, and convection with blood. When the temperature reaches 39°C, the threshold to trigger thermoregulatory response,
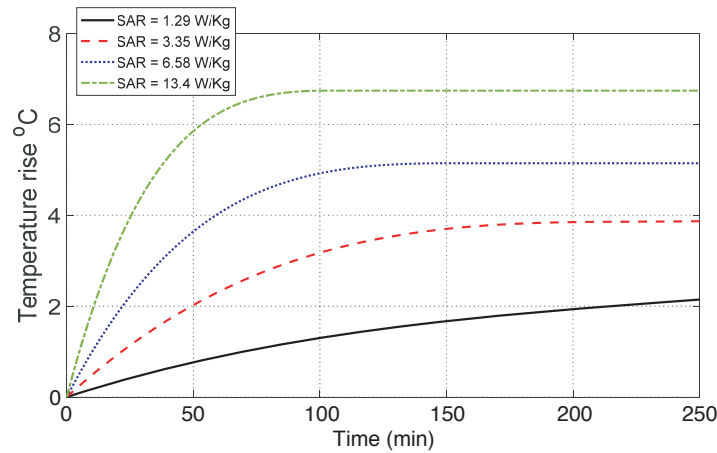
Figure 19. Temperature rise with time for bone tissues subjected to different values of SAR.
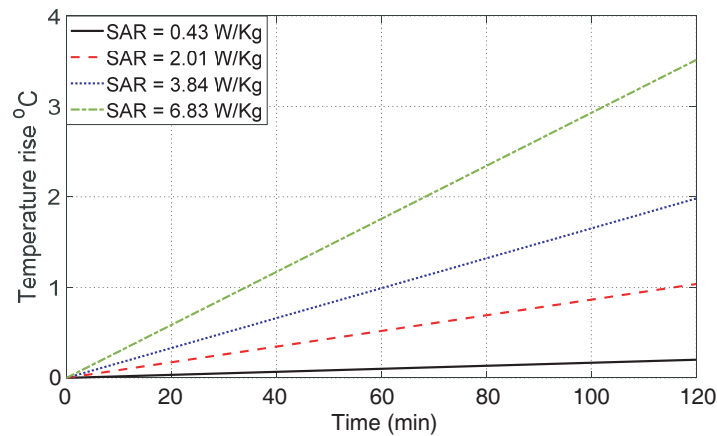
Figure 20. Temperature rise with time for synovial fluid subjected to different values of SAR.

the increased rate of blood flow tends to increase the cooling rate of the tissue.

In the cases of bone, muscle, fat, cartilage, and ligament, the cooling mechanisms utilized by the tissue to reach a steady state temperature are convection via blood and conduction to neighbouring tissues. For skin, the rise in tissue temperature in all the cases investigated is not enough to trigger thermoregulatory response (the skin initial temperature is lower than the rest of the tissues), but heat loss by radiation, convection with blood and air, and evaporation could efficiently cool the skin under the selected exposure conditions.

In the case of body fluid, there is no blood supply to the fluid; therefore, the fluid does not lose heat to blood by convection. Radiation and evaporation are blocked by the surrounding tissue. Conduction to the surrounding tissue is the only mechanism available for heat dissipation. Thus, body fluid does not reach steady state in any of the applied exposure conditions. This can be clearly seen in Figure 20, for the synovial fluid.

5.7. Steady State Temperature Rise versus SAR

This section depicts the relationship between the absorbed SAR and the steady state rise in tissue temperature (ΔT_s) for each tissue type individually. The source of microwave radiation (the dipole) is located at the position indicated in Figure 1(b), and the values of SAR and temperature are evaluated. Figure 21 shows the relationship between the steady state rise in tissue temperature and the local SAR at a point in the muscle tissue. Cartilage and tendon are found to have the same behaviour.
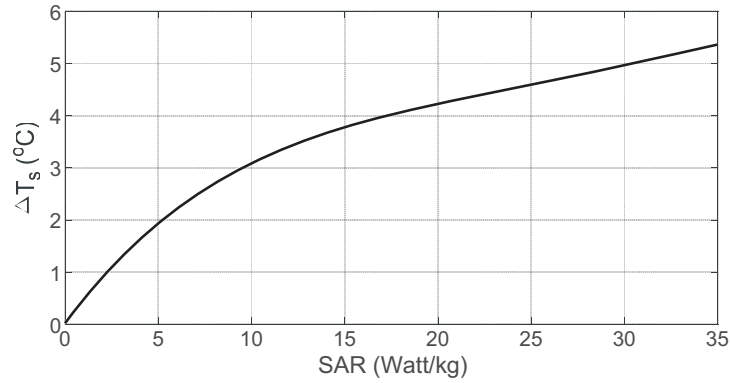
Figure 21. The relationship between (ΔT_s) and local SAR inside a point in the muscle tissue.

The steady state temperature rise versus the SAR in the skin is presented in Figure 22.
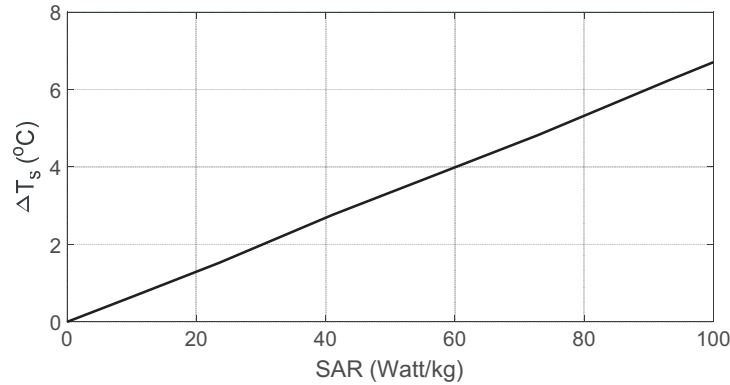
Figure 22. Steady state rise in tissue temperature versus SAR for skin.
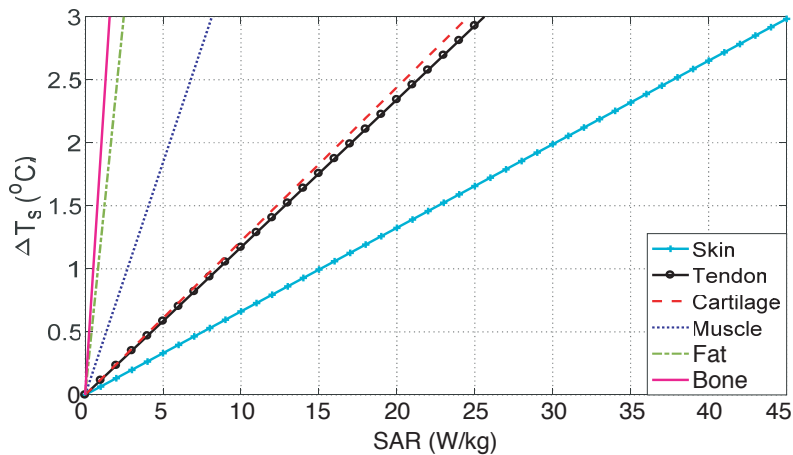
Figure 23. Linear relation between steady state rise in tissue temperature and SAR for tendon, cartilage, skin, bone, fat and muscle.

From the results presented so far, the relationship between the steady state rise in tissue temperature and SAR is always linear for temperatures below 39°C. Above this temperature, the linear relationship is disturbed. However for the skin, the relationship is linear throughout the entire range

of SAR values because the skin initial temperature is low (as mentioned earlier), thus, the final steady state temperature does not exceed 39°C in any of the investigated exposure conditions.

The slope (χ) between the SAR and the rise in temperature measured in (°C kg/W) is of crucial importance for the linear part of the relation. It can be considered as a measure of the susceptibility of tissue to be heated by electromagnetic radiation at the applied frequency. Figure 23 compares the linear part of the relationship between the steady rise in tissue temperature and the SAR for the muscle, tendon, skin, cartilage, fat, and bone in one plot. The value of χ for a specific tissue may be affected by the structure of the surrounding tissue. The bone and fat are the tissue types with the highest susceptibility to heating, and this is why during diathermy treatment, hot spots may arise inside the fat tissue when the covering skin is still at a safe temperature. Tissues are arranged according to values of the slope, χ, and shown in Table 3.

Table 3. The values of χ for different tissue types.

Tissue	Slope χ (°C kg/W)
Bone	1.653
Fat	1.320
Muscle	0.373
Cartilage	0.1211
Tendon	0.114
Skin	0.0661

5.8. Steady State Temperature versus Averaged SAR for Muscle Tissue

The SAR values averaged over 1 g (SAR_{1g}) and over 10 g (SAR_{10g}) have been computed considering tissue masses in the shape of a cube. To obtain the relationship between the steady state temperature at a point and each of the SAR averaged over 1 g and 10 g, a cubic volume is taken in the tissue with its centre at the point of calculation. Cubes weighing 0.9 grams for SAR_{1g} and 9 grams for SAR_{10g} have been examined. It should be noted that the applied input powers to the antenna are small enough to ensure that thermoregulatory responses are not triggered inside the tissue. The dipole is located as indicated in Figure 1(b). Examples for the relationship between the steady state temperature rise and the averaged SAR are shown in Figure 24 for the muscle tissue.
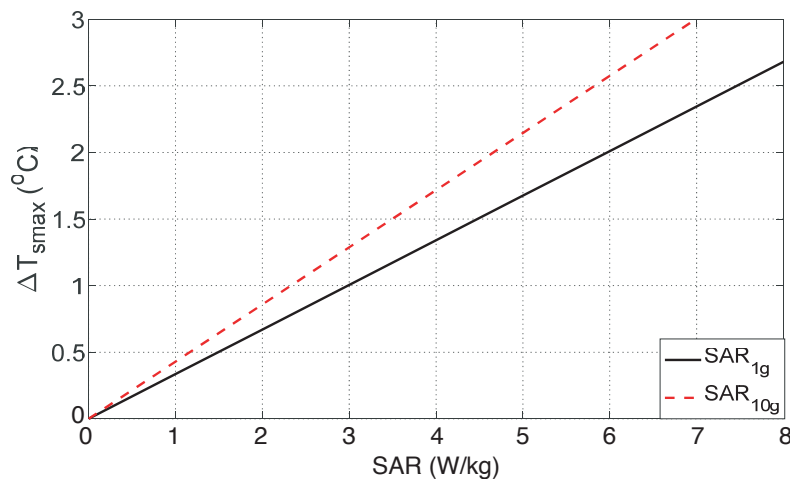
Figure 24. The relation between (ΔT_S) and each of SAR_{1g} and SAR_{10g} for low SAR values in the muscle tissue of the knee.

At the thermal steady state, it could be appropriate to express the maximum temperature increase in biological tissue as a function of the averaged SAR by the following equation:

$$\Delta T_{s_{\max}} \leq \alpha \mathrm{SAR}_{\mathrm{avg}} \tag{13}$$

where $\mathrm{SAR}_{\mathrm{avg}}$, $\Delta T_{s_{\max}}$, and α denote the SAR averaged over 1 or $10\,\mathrm{g}$ of the tissue, the maximum temperature rise, and the slope of the line in units of $(\degree\mathrm{C} \cdot \mathrm{kg})/\mathrm{W}$, respectively. Note that no temperature increase in the knee is induced without electromagnetic power absorption. Slope α can be denoted as the
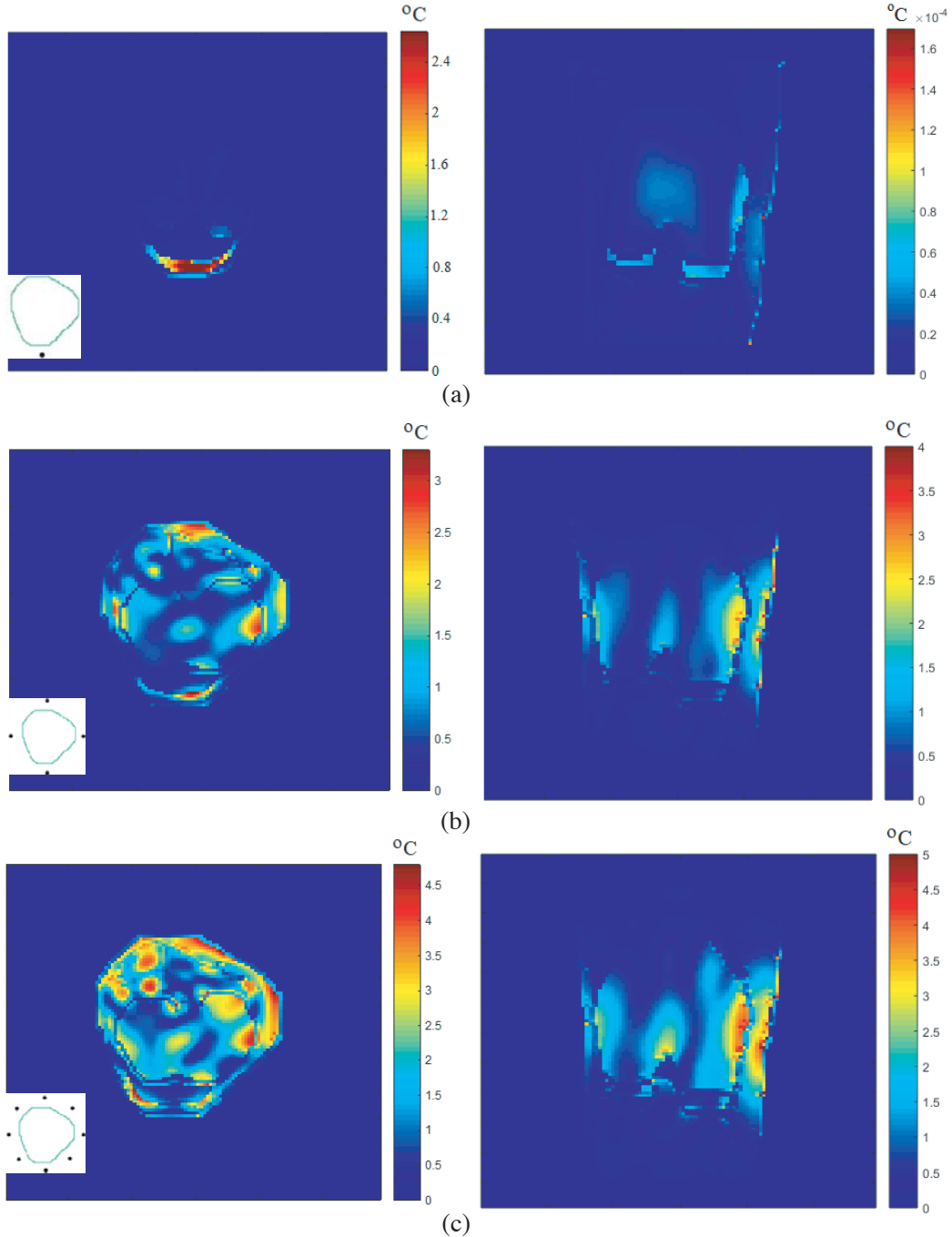
Figure 25. Temperature rise distribution in the middle axial cross section (left column) and middle sagittal cross section (right column) due to (a) single dipole, (b) circular array of four dipoles, (c) circular array of 8 dipoles.

normalized heating factor [24]. For $SAR_{1\,g}$, slope α is obtained from the simulations, and Equation (13) is written as,

$$\Delta T_{s_{\max}} \leq 0.3345 SAR_{1\,g} \qquad (14)$$

and for $SAR_{10\,g}$, Equation (13) is written as,

$$\Delta T_{s_{\max}} \leq 0.4298 SAR_{10\,g} \qquad (15)$$

Slope α computed in either relation is not a constant value for the muscle tissue. The slope depends greatly on the selected part of the muscle tissue for evaluation, i.e., on the intervening and surrounding tissues. On the basis of these results, it is necessary to specify a more accurate value of slope α correlating the maximum temperature increase with the averaged SAR. This would be accomplished by using much more samples for the averaged SAR values and the maximum temperature increase.

The work of [31] stated that the correlations between the maximum temperature increase and the averaged SAR are not dependent on the EM wave frequency, although the electrical constants of tissues are largely dependent on the frequency.

5.9. Distribution of Temperature Rise

This section is concerned with the presentation and discussion of the steady-state temperature rise distribution in the different tissues around the knee joint as a consequence of being subjected to electromagnetic exposure from single dipole antenna and circular arrays of four and eight dipoles. Color scale plots for the temperature rise distribution in the axial and sagittal cross sections of the knee are presented. The plots summarize the results concerned with the temperature rise in the different tissue types around the knee joint which is extensively discussed in the previous sections. Figures 25(a), (b), and (c) show the temperature rise distribution due to radiation from a single dipole, circular array of four dipoles, and circular array of eight dipoles, which correspond to the steady-state SAR distributions presented in Figures 6, 9, and 11, respectively. Each dipole is excited with a sinusoidal voltage signal of magnitude 10 V and frequency 2.45 GHz applied across an infinitesimal gap at the dipole centre. It can be seen in the figures that with increasing the number of dipoles the temperature rise globally increases, and its distribution becomes more homogeneous. Also, it can be seen that the maximum temperature rise is about 5°C in the case of circular array of eight dipoles, which is still in the safe range (≤ 42°C) that will not affect the tissues negatively or cause burning or hot spots.

6. CONCLUSION

In this work, a thermotherapy device composed of a circular array of dipoles is proposed for the treatment of the human knee disorders. A three-dimensional model of the knee is constructed using two-dimensional images for a number of cross sections taken regularly along the knee. The FDTD is applied to calculate the SAR distribution within the knee tissues due to electromagnetic radiation from the circular array. The maximum SAR has increased in the case of 8 dipoles. The temperature rise in the different tissues is obtained by applying the FDTD method to the BHE. In solving the thermal problem, we attempt to apply the most realistic boundary conditions. A complete thermal model of the human body has been implemented. The forward divided difference and centered divided difference are used to solve for the first and second order derivatives of the BHE, respectively. Convective, radiative, and evaporative boundary conditions are applied. The effect of the thermoregulatory system has been considered as well.

The relationship between the temperature rise and the SAR value is studied for each tissue type in the knee using a single dipole radiating at different power levels. The results of temperature increase due to microwave exposure show that the presence of the thermoregulatory system strongly limits the temperature elevations. If thermoregulation is inhibited, a relevant increase in the blood temperature is induced. Therefore, even if power absorption is limited to one body region, temperature elevations will occur throughout the body.

The time taken for the electric field to reach steady state inside biological tissue is rather short, in the order of 10^{-9} sec in the examined exposure conditions, whereas the time required for the tissue to reach steady temperature is about 20 min for the applied boundary conditions. Many parameters are

computed based on the values of the steady state rise in tissue temperature (ΔT_s). It should be noted that the steady state temperature is often reached after prolonged exposure duration for many exposure conditions; for example during a diathermy session or a mobile phone call. It is therefore interesting to consider the time evolution of the temperature. The local and averaged SAR values deposited in the muscle tissues are linearly dependent on the average power incident on the knee. The results also reveal the linear dependence of the rise in tissue temperature (up to 39°C) on the averaged power incident on the knee.

REFERENCES

1. National Health and Medical Research Council *Code of Practice for the Safe use of Microwave Diathermy Units*, Reprinted from the Report of the 99th Session of the Council, June 1985.

2. Hirata, A., H. Sugiyama, and O. Fujiwara, "Estimation of core temperature elevation in humans and animals for whole-body averaged SAR," *Progress In Electromagnetics Research*, Vol. 99, 53–70, 2009.

3. Trujillo-Romero, C. J., S. Garcia-Jimeno, A. Vera, L. Leija, and J. Estelrich, "Using nanoparticles for enhancing the focusing heating effect of an external waveguide applicator for oncology hyperthermia: Evaluation in muscle and tumor phantoms," *Progress In Electromagnetics Research*, Vol. 121, 343–363, 2011.

4. Singh, S. P., "Microwave thermotherapy and its clinical applications," URSI AP-RASC, March 2019.

5. Imaiyutaka, B. S., T. Ohigashi, H. Tazaki, and Y. Imai, "Transurethral microwave thermotherapy for benign prostatic hyperplasia," *J. Urol.*, Vol. 6, 371–373, 1992.

6. Vrbova, B. and J. Vrba, "Microwave thermotherapy in cancer treatment: Evaluation of homogeneity of SAR distribution," *Progress In Electromagnetics Research*, Vol. 129, 181–195, 2012.

7. Gas, P., "Temperature distribution of human tissue in interstitial microwave hyperthermia," *Przegl Elektrotechniczny (Electrical Review)*, ISSN 0033-2097, R. 88 NR 7a, 2012.

8. Rabini, A., D. B. Piazzini, G. Tancredi, C. Foti, G. Milano, G. Ronconi, A. Specchia, P. E. Ferrara, L. Maggi, E. Amabile, and M. Galli, "Deep heating therapy via microwave diathermy relieves pain and improves physical function in patients with knee osteoarthritis: A double-blind randomized clinical trial," *Eur. J. Phys. Rehabil. Med.*, Vol. 48, No. 4, 549–559, 2012.

9. Hamed, T. and M. Maqsood, "SAR calculation and temperature response of human body exposure to electromagnetic radiations at 28, 40, and 60 GHz mm wave frequencies," *Progress In Electromagnetics Research M*, Vol. 73, 47–59, 2018.

10. Nyborg, W. L., "Solutions of the bio-heat transfer equation," *Phys. Med. Biol.*, Vol. 33, No. 7, 785–792, 1988.

11. Damor, R. S., S. Kumar, and A. K. Shukla, "Numerical solution of fractional bioheat equation with constant and sinusoidal heat flux condition on skin tissue," *American Journal of Mathematical Analysis*, Vol. 1, No. 2, 20–24, 2013.

12. Jorge, M. S. G., C. Zanin, B. Knob, and L. M. Wibelinger, "Effects of deep heating to treat osteoarthritis pain: Systematic review," *Sociedade Brasileira para o Estudo da Dor*, Vol. 18, No. 1, 79–84, 2017.

13. Abinzano, I. F., "Induced hyperthermia in promoting cartilage regeneration," Master of Science in Biomedical Engineering, Delft University of Technology, 2016.

14. Gabriel, S., R. W. Lau, and C. Gabriel, "The dielectric properties of biological tissues: II. Measurements in the frequency range 10 Hz to 20 GHz," *Phys. Med. Biol.*, Vol. 41, No. 11, 2251–2269, November 1996.

15. Musa, B. U., "Implementation of unsplit perfectly matched layer absorbing boundary condition in 3 dimensional finite difference time domain method," *Arid Zone Journal of Engineering, Technology and Environment*, Vol. 13, No. 2, 238–251, April 2017.

16. Mäkinen, R. M., J. S. Juntunen, and M. A. Kivikoski, "An improved thin-wire model for FDTD," *IEEE Microwave Theory and Techniques*, Vol. 50, No. 5, 1245–1255, May 2002.

17. Cherry, P. and M. Iskander, "Calculations of heating patterns of an array of microwave interstitial antennas," *IEEE Trans. on Biomedical Engineering*, Vol. 40, No. 8, 771–779, August 1993.

18. Hoque, F. and O. Ghandhi, "Temperature distributions in the human leg for VLF-VHF exposure at the ANSI recommended safety levels," *IEEE Trans. on Biomedical Engineering*, Vol. 35, No. 6, 442–449, June 1988.

19. Zolfaghari, A. and M. Maerefat, *Developments in Heat Transfers*, Chapter 9 Bioheat Transfer, InTech Press, 2011.

20. Kottke, F. and F. Lehmann, *Kruse's Handbook of Physical Medicine and Rehabilitation*, W. B. Saunders, 1990.

21. Pandolf, B. and E. Burr, "Medical aspects of harsh environments," Office of the Surgeon General at TMM Publications, Vol. 1, 2001.

22. USAF School of Aerospace Medicine, *Radiofrequency Radiation and Dosimetry Handbook*, Aerospace Medical Division (AFSC), Brooks Air Force Base, TX 78235-5301, June 1997.

23. Inouye, T. F. Hick, E. Tesler, and R. Keetan, "Effect of relative humidity on heat loss of men exposed to environments of 80, 76 and 72°F," *Amer. Soc. Heating, Referigerating, Air Conditioning Eng. Trans.*, Vol. 59, 59, 1953.

24. Bernardi, P., M. Cavagnaro, S. Pisa, and E. Piuzzi, "Specific absorption rate and temperature increases in the head of a cellular-phone user," *IEEE Trans. on Microwave Theory and Techniques*, Vol. 48, No. 48, 1118–1126, July 2000.

25. Yioultsis, T., T. Kosmanis, E. Kosmidou, T. Zygiridis, N. Kantartziz, T. Xenos, and T. Tsiboukis, "A comparative study of the biological effects of the various mobile phone and wireless LAN antennas," *IEEE Trans. on Magnetics*, Vol. 38, No. 2, 777–780, March 2002.

26. Bernardi, P., M. Cavagnaro, S. Pisa, and E. Piuzzi, "Specific absorption rate and temperature elevation in a subject exposed in the far-field of a radiofrequency sources operating in the 100–900-MHz," *IEEE Trans. on Biomedical Engineering*, Vol. 50, No. 3, 295–204, March 2003.

27. Rossmann, C. and D. Haemmerich, "Review of temperature dependence of thermal properties, dielectric properties, and perfusion of biological tissues at hyperthermic and ablation temperatures," *Advances in Science, Technology and Engineering Systems Journal*, Vol. 42, No. 6, 467–492, 2014.

28. Hirata, A., M. Morita, and T. Shiozawa, "Temperature increase in the human head due to dipole antenna at microwave frequencies," *IEEE Trans. on Electromagnetic Compatibility*, Vol. 45, No. 1, 109–116, February 2003.

29. Li, Q.-X. and O. Ghandhi, "Thermal implications of the new relaxed IEEE RF safety standard for head exposures to cellular telephones at 835 and 1900 MHz," *IEEE Trans. on Microwave Theory and Techniques*, Vol. 54, No. 7, 3146–3154, July 2006.

30. Luitel, K., D. B. Gurung, and K. N. Uprety, "Effect of various parameters for temperature distribution in human body: An analytic approach," *Advances in Science, Technology and Engineering Systems Journal, Special issue on Recent Advances in Engineering Systems Journal*, Vol. 3, No. 5, 421–426, 2018.

31. Fujimoto, M., A. Hirata, J. Wang, O. Fujiwara, and S. Toshiyuki, "FDTD-derived correlation of maximum temperature increase and peak SAR in child and adult head models due to dipole antenna," *IEEE Trans. on Electromagnetic Compatibility*, Vol. 48, No. 1, 240–247, February 2006.